Self-Consistent Field Theory of Polyelectrolyte Systems†

Qiang Wang,‡ Takashi Taniguchi,§ and Glenn H. Fredrickson*,‡

Department of Chemical Engineering and the Materials Research Laboratory, University of California−Santa Barbara, Santa Barbara, California 93106, and Department of Polymer Science and Engineering, Yamagata University, 3-4-16, Yonezawa, Yamagata, 992-8510, Japan

Received: October 9, 2003; In Final Form: January 6, 2004

A self-consistent field theory is applied to inhomogeneous polyelectrolyte systems. We consider the smeared and the annealed charge distributions, corresponding to strongly and weakly dissociating polymers, respectively. The electrostatic interactions are described by the nonlinear Poisson−Boltzmann equation, where the dielectric constant of the system is treated as position-dependent to take into account the large difference between those of hydrophobic polymers and water-like solvents. We present results for several systems, including the interface of a phase-separated polyelectrolyte solution in a poor solvent, the lamellar structures of symmetric diblock polyelectrolytes, and the phase behavior of polyelectrolyte blends.

1. Introduction

Despite their great interest in biological and industrial applications, polyelectrolytes remain among the least understood polymeric systems.[1] The difficulty lies in the existence of long-range Coulomb interactions in addition to short-range excluded volume interactions in the system. There are many controlling parameters, and experimental systems are quite sensitive to salt concentration, solution pH, etc. The long-range interactions also make molecular simulations difficult, where computationally expensive techniques (e.g., Ewald sums[2]) have to be employed. Very recently, field-theoretic simulations (FTS) were proposed, which allow sampling of fluctuations in the system of interest and thus extend current mean-field self-consistent field (SCF) theory.[3,4] In the FTS (and the SCF theory), a long-range Coulomb interaction becomes a short-range interaction after the Hubbard−Stratonovich transformation that introduces the electrostatic potential into the partition function;[4] it might therefore be easier to study polyelectrolyte systems using FTS than using particle-based simulations. As the first step along this line, in this work we apply the SCF theory to polyelectrolyte systems.

The SCF theory for polymers, originated by Edwards[5] and by Helfand and Tagami,[6] has been widely applied to and gained great success in inhomogeneous neutral polymer systems, including interfaces of polymer blends,[6,7] microphase separation of block copolymers,[8,9] polymers near surfaces,[10] etc.[11] It, however, has rarely been applied to polyelectrolyte systems. Under the ground state dominance approximation valid in certain special cases, Borukhov et al. applied the SCF theory to semidilute solutions of polyelectrolytes and polyampholytes having various charge distributions.[12] Their theory has also been used to study polyelectrolyte adsorption.[13] Recently, Shi and Noolandi established the SCF formalism for multicomponent polyelectrolyte solutions, and derived the asymptotic forms of the theory at weak and strong segregation limits.[14] They also studied as a simple example the interface of a phase-separated polyelectrolyte solution in a poor solvent, where the polyelectrolytes had the smeared charge distribution.[14]

Different from the above work where the dielectric constant of the system was constant, we treat it as position-dependent by coupling it with local densities of the polyelectrolytes and the solvent. The presence of a polar solvent (e.g., water) is essential for polyelectrolyte segments to dissociate and release counterions. The dielectric constants of organic polymers (e.g., polystyrene) and the solvent, however, could differ by 1 or 2 orders of magnitude. This needs to be taken into account, especially for strongly inhomogeneous systems. Our theoretical formalism is presented in section 2, where both the smeared and the annealed charge distributions are considered. In section 3 we apply the SCF theory to several polyelectrolyte systems, to demonstrate the capability of our formalism and to present new results on these systems. We first in section 3.1 study the interface of a phase-separated polyelectrolyte solution in a poor solvent and determine the one-dimensional density profiles across the (flat) interface. This serves as a simple example to understand the effects of various parameters in our theory (e.g., charge distributions, dielectric constants, salt concentration, etc.).

We then in section 3.2 study the lamellar structure of symmetric diblock polyelectrolytes A−B (where the only difference between A and B is that they carry opposite charges) in a good solvent. Similar to neutral block copolymers, block polyelectrolytes also undergo order−disorder transitions (ODT) and form various microphase-separated structures. However, the charges in general make different blocks more compatible, and introduce new controlling parameters (e.g., degrees of ionization, charge distributions, dielectric constants) into the system. This could change and even generate new ordered morphologies. Theoretical study of microphase separation of block polyelectrolytes, however, has been limited to the random phase approximation (RPA) analysis on diblocks having the smeared charge distribution.[15−20] In these studies, the structure matrix of the homogeneous phase was constructed from the expansion of its free energy in terms of density fluctuations to the second order; the ODT temperature and the corresponding period of the microphase were then obtained by solving the generalized spinodal equations.[15−20] The ordered structures below the ODT, however, have not been studied theoretically. For such systems, the ground state dominance approximation is clearly not valid. Recently, Banaszak and Clarke performed molecular dynamics

† Part of the special issue "Hans C. Andersen Festschrift".
* Corresponding author.
‡ University of California−Santa Barbara.
§ Yamagata University.

10.1021/jp037053y CCC: $27.50
Published on Web 04/27/2004

simulations of diblock polyelectrolytes with the charged block A consisting of 16 segments and the neutral block B of 15 segments; every other segment in the A blocks carries an elementary charge, and eight couterions (for each chain) of the same size as chain segments are explicitly included in the system.[21] Due to counterion condensation, which increases the effective volume fraction of the A blocks, perforated lamellae were obtained below the ODT.[21]

Microphase separation can also occur in polyelectrolyte solutions and blends; this is different from their neutral counterparts where only macroscopic phase separation occurs. We therefore in section 3.3 study the lamellar structure and the competition between the macroscopic phase separation and the microphase separation of polyelectrolyte blends A/B, with A and B having the same chain length. Microphase separation of polyelectrolyte solutions was first predicted by Borue and Erukhimovich,[22] and that of polyelectrolyte blends was first studied independently by Nyrkova et al.,[23] by Brereton and Viglis,[24] and by Joanny and Leibler.[25] The aforementioned RPA-type analysis has been applied in most theoretical studies on microphase separation of polyelectrolyte solutions and blends.[12,16,20,22−31] Since in these studies, as well as in those for block polyelectrolytes, the annealed charge distribution has rarely been treated,[12] we derive the RPA results from our theory for both the smeared and the annealed charge distributions in the Appendix; for symmetric polyelectrolyte blends, simplified results focusing on the effects of dielectric constants are also derived. By expanding the free energy of the homogeneous phase to the fourth order (as in Leibler's work on microphase separation of neutral block copolymers[32]), Erukhimovich and co-workers constructed mean-field phase diagrams of polyelectrolyte solutions[22,26,33] and blends[34] in the weak segregation regime; in the latter case fluctuation corrections under the Brazovskii approximation were also reported.[34] By direct minimization of a square-gradient free-energy functional, Nyrkova et al. studied the lamellar structures below the ODT and the competition between the macroscopic phase separation and the microphase separation of polyelectrolyte blends and solutions.[35] Note, however, that their free-energy functional is not uniformly valid at all temperatures below the ODT[36] and cannot be applied to block copolymers.[35] Also, the accuracy of their calculations was poor at low temperatures, which led to incorrect phase diagrams. We therefore revisit their phase diagrams for blends of charged and neutral polymers A/B at the end of section 3.3. The last section is devoted to conclusions.

2. Theoretical Formalism

2.1. Charged Homopolymers in Solution. Here we consider charged homopolymers in a solution of small-molecule solvent S with presence of salt. Each polymer chain of type P (= A, B, ...) has N_P segments. We assume that all polymer segments have the same density ρ_0 as solvent molecules, and ignore the volume of small ions. We also assume that the counterions from polyelectrolytes are identical to the ions from salt that carry the same type of charge, and denote cations by + and anions by −. Integer variables $v_+ > 0$, $v_- < 0$, and v_P are used to denote the increments of unit charge e carried by cations, anions, and the P polymer segments, respectively. In a canonical ensemble at volume V and temperature T (hereafter we set $k_BT = 1$ where k_B is the Boltzmann constant), the partition function of the system is

$$\mathcal{Z} = \prod_j \frac{1}{n_j!} \prod_{\mathrm{P}} \prod_{k=1}^{n_\mathrm{P}} \int \mathcal{D}\mathbf{R}_{\mathrm{P},k} \prod_{\mathrm{M}} \prod_{k=1}^{n_\mathrm{M}} \int \mathrm{d}\mathbf{r}_{\mathrm{M},k} \int \mathcal{D}\psi \times \prod_{\mathrm{P}} \prod_{k=1}^{n_\mathrm{P}} \sum_{\{\theta_{\mathrm{P},k}(s)\}} \exp(-\mathscr{H})\, \delta\left(\int \mathrm{d}\mathbf{r}\hat{\rho}_e(\mathbf{r})\right) \prod_{\mathbf{r}} \delta\left(\sum_{\mathrm{P}} \hat{\rho}_{\mathrm{P}}(\mathbf{r}) + \hat{\rho}_{\mathrm{S}}(\mathbf{r}) - \rho_0\right) \quad (1)$$

where j represents all the species in the system and M represents only the small-molecule species (i.e., S, +, and −); n_j denotes the number of molecules of species j; $\mathbf{R}_{\mathrm{P},k}$ represents the space curve of the kth chain of type P and $\mathbf{r}_{\mathrm{M},k}$ denotes the spatial position of the kth molecule of species M; and $\psi(\mathbf{r})$ denotes the electrostatic potential at position $\mathbf{r}$. In eq 1, $\theta_{\mathrm{P},k}(s)$ represents the dissociation of the sth segment of the kth chain of type P. If we denote the degree of ionization of the P polymer by $\alpha_P \in [0, 1]$, then for the smeared charge distribution (corresponding to strongly dissociating polyelectrolytes) $\theta_{\mathrm{P},k}(s) = \alpha_P$; for the annealed charge distribution (corresponding to weakly dissociating polyelectrolytes), $\theta_{\mathrm{P},k}(s)$ is a two-state variable with 1 corresponding to a dissociated segment and 0 to a nondissociated segment, and these two states are weighted by α_P and $1 - \alpha_P$, respectively (in addition to the Boltzmann factor).[37] Also in eq 1, the Hamiltonian of the system consists of three parts: $\mathscr{H} \equiv \mathscr{H}_0 + \mathscr{H}_1 + \mathscr{H}_2$, where

$$\mathscr{H}_0 = \sum_{\mathrm{P}} \sum_{k=1}^{n_\mathrm{P}} \frac{3}{2a^2} \int_0^{N_\mathrm{P}} \mathrm{d}s(\dot{\mathbf{R}}_{\mathrm{P},k}(s))^2 \quad (2)$$

describes the elastic energy of Gaussian chains, where a is the statistical segment length (assumed to be the same for all chains), and $\dot{\mathbf{R}}_{\mathrm{P},k}(s)$ denotes $\mathrm{d}\mathbf{R}_{\mathrm{P},k}(s)/\mathrm{d}s$;

$$\mathscr{H}_1 = \frac{1}{\rho_0} \sum_{\mathrm{P}} \int \mathrm{d}\mathbf{r}\hat{\rho}_{\mathrm{P}}(\mathbf{r}) \left[\chi_{\mathrm{PS}}\hat{\rho}_{\mathrm{S}}(\mathbf{r}) + \frac{1}{2}\sum_{\mathrm{P}' \neq \mathrm{P}} \chi_{\mathrm{PP}'}\hat{\rho}_{\mathrm{P}'}(\mathbf{r})\right]$$

describes the short-range (e.g., van der Waals) interaction energy of the system, where χ_{PS} is the Flory−Huggins interaction parameter between the polymer segments of type P and the solvent molecules, and $\chi_{PP'}$ is that between the polymer segments of type P and those of type P′; and

$$\mathscr{H}_2 = \int \mathrm{d}\mathbf{r}\hat{\rho}_e(\mathbf{r})\psi(\mathbf{r}) - \frac{\epsilon(\mathbf{r})}{8\pi e^2}|\nabla\psi(\mathbf{r})|^2 \quad (3)$$

describes the electrostatic energy of the system, where $\epsilon(\mathbf{r})$ is the dielectric constant at $\mathbf{r}$ (in units of $4\pi\epsilon_0$, where $\epsilon_0 = 8.85 \times 10^{-12}$ (A·s)^2/(J·m) is the permittivity of vacuum), and $\hat{\rho}_e(\mathbf{r})$ is the total charge density (in units of e) at $\mathbf{r}$.[40] Note that $\psi(\mathbf{r})$ (in units of k_BT/e) is pure imaginary in this notation. The first δ function in eq 1 corresponds to the charge neutrality of the whole system, and the second one imposes the incompressibility at all $\mathbf{r}$. The microscopic densities in the above equations are defined as

$$\hat{\rho}_{\mathrm{P}}(\mathbf{r}) \equiv \sum_{k=1}^{n_\mathrm{P}} \int_0^{N_\mathrm{P}} \mathrm{d}s\delta(\mathbf{r} - \mathbf{R}_{\mathrm{P},k}(s)) \quad (4)$$

$$\hat{\rho}_{\mathrm{M}}(\mathbf{r}) \equiv \sum_{k=1}^{n_\mathrm{M}} \delta(\mathbf{r} - \mathbf{r}_{\mathrm{M},k}) \quad (5)$$

$$\hat{\rho}_e(\mathbf{r}) \equiv \sum_{\mathrm{P}} \left[v_{\mathrm{P}} \sum_{k=1}^{n_\mathrm{P}} \int_0^{N_\mathrm{P}} \mathrm{d}s\theta_{\mathrm{P},k}(s)\delta(\mathbf{r} - \mathbf{R}_{\mathrm{P},k}(s))\right] + v_+\hat{\rho}_+(\mathbf{r}) + v_-\hat{\rho}_-(\mathbf{r}) \quad (6)$$

We define the normalized densities $\hat{\phi}_j(\mathbf{r}) \equiv \hat{\rho}_j(\mathbf{r})/\rho_0$ and insert in eq 1 the following identity:

$$1 = \prod_j \int \mathcal{D}\phi_j \mathcal{D}\omega_j \exp\{\rho_0 \int d\mathbf{r}\omega_j(\mathbf{r})[\phi_j(\mathbf{r}) - \hat{\phi}_j(\mathbf{r})]\}$$

where $\phi_j(\mathbf{r})$ is a density field constrained to $\hat{\phi}_j(\mathbf{r})$ and $\omega_j(\mathbf{r})$ (which is pure imaginary) is a conjugate field interacting with species j that imposes the constraint. Next, we substitute eqs 4−6 into the above identity, and the following integral form of the two δ functions into eq 1:

$$\delta\left(\int d\mathbf{r}\hat{\rho}_e(\mathbf{r})\right) = \int d\lambda \exp\{-\lambda \int d\mathbf{r}[\sum_P [v_P \sum_{k=1}^{n_P} \times \int_0^{N_P} ds\theta_{P,k}(s)\delta(\mathbf{r} - \mathbf{R}_{P,k}(s))] + \rho_0(v_+\phi_+(\mathbf{r}) + v_-\phi_-(\mathbf{r}))]\} \quad (7)$$

$$\prod_{\mathbf{r}} \delta(\rho_0[\sum_P \phi_P(\mathbf{r}) + \phi_S(\mathbf{r}) - 1]) = \int \mathcal{D}\eta \exp\{-\int d\mathbf{r}\eta(\mathbf{r})\rho_0[\sum_P \phi_P(\mathbf{r}) + \phi_S(\mathbf{r}) - 1]\}$$

where the Lagrange multipliers λ and $\eta(\mathbf{r})$ (which are pure imaginary) are introduced. One then sees that λ can be absorbed into $\psi(\mathbf{r})$, i.e., $\int \mathcal{D}\psi \int d\lambda f(\psi(\mathbf{r}) + \lambda) \propto \int \mathcal{D}\psi f(\psi(\mathbf{r}))$ for any function f. Also, if we assume that $\{\theta_{P,k}(s)\}$ are independently distributed, the term containing the summation over $\theta_{P,k}(s)$ for all the segments on a chain can then be directly evaluated as

$$\sum_{\{\theta_{P,k}(s)\}} \exp[-v_P \int_0^{N_P} ds\theta_{P,k}(s)\psi(\mathbf{R}_{P,k}(s))] = \exp[\int_0^{N_P} ds g_P(\mathbf{R}_{P,k}(s))]$$

where $g_P(\mathbf{r}) \equiv -\alpha_P v_P \psi(\mathbf{r})$ for the smeared case, and $g_P(\mathbf{r}) \equiv \ln[1 - \alpha_P + \alpha_P \exp(-v_P\psi(\mathbf{r}))]$ for the annealed case. The partition function can finally be written as

$$\mathcal{Z} = \int \prod_j (\mathcal{D}\phi_j \mathcal{D}\omega_j) \mathcal{D}\psi \mathcal{D}\eta \exp(-\mathcal{F})$$

$$\frac{\mathcal{F}}{\rho_0} = \int d\mathbf{r}\left\{\sum_P \left[\chi_{PS}\phi_S(\mathbf{r}) + \frac{1}{2}\sum_{P'\neq P} \chi_{PP'}\phi_{P'}(\mathbf{r}) + \eta(\mathbf{r}) - \omega_P(\mathbf{r})\right]\phi_P(\mathbf{r}) + [\eta(\mathbf{r}) - \omega_S(\mathbf{r})]\phi_S(\mathbf{r}) - \eta(\mathbf{r}) + [v_+\psi(\mathbf{r}) - \omega_+(\mathbf{r})]\phi_+(\mathbf{r}) + [v_-\psi(\mathbf{r}) - \omega_-(\mathbf{r})]\phi_-(\mathbf{r}) - \frac{\epsilon(\mathbf{r})}{8\pi\rho_0 e^2}|\nabla\psi(\mathbf{r})|^2\right\} - V\left(\sum_P \frac{\bar{\phi}_P}{N_P} \ln\frac{Q_P}{\bar{\phi}_P} + \sum_M \bar{\phi}_M \ln\frac{Q_M}{\bar{\phi}_M}\right) \quad (8)$$

where the volume-averaged densities $\bar{\phi}_P \equiv n_P N_P/(\rho_0 V)$ and $\bar{\phi}_M \equiv n_M/(\rho_0 V)$, and

$$Q_P \equiv \frac{\int \mathcal{D}\mathbf{R} \exp\left\{-\int_0^{N_P} ds \left[\frac{3}{2a^2}(\dot{\mathbf{R}}(s))^2 + \omega_P(\mathbf{R}(s)) - g_P(\mathbf{R}(s))\right]\right\}}{\int \mathcal{D}\mathbf{R} \exp\left\{-\int_0^{N_P} ds \frac{3}{2a^2}(\dot{\mathbf{R}}(s))^2\right\}} \quad (9)$$

$$Q_M \equiv \frac{1}{V}\int d\mathbf{r} \exp[-\omega_M(\mathbf{r})]$$

Note that to obtain eq 8 the Stirling approximation $\ln(n_j!) \approx n_j(\ln n_j - 1)$ is used and a constant is added to $\mathcal{F}$.

The mean-field SCF equations are obtained by the saddle-point approximation, where one sets $\delta\mathcal{F}/\delta\phi_j(\mathbf{r}) = 0$, $\delta\mathcal{F}/\delta\omega_j(\mathbf{r}) = 0$, $\delta\mathcal{F}/\delta\psi(\mathbf{r}) = 0$, and $\delta\mathcal{F}/\delta\eta(\mathbf{r}) = 0$. If we denote the radius of gyration of a Gaussian chain of N segments by $R_g \equiv a\sqrt{N/6}$ and rescale variables according to $\mathbf{r}/R_g \to \mathbf{r}$ (thus $V/R_g^d \to V$ where d is the dimensionality of the system), $s/N \to s$, $N\omega_j(\mathbf{r}) \to \omega_j(\mathbf{r})$, $N\eta(\mathbf{r}) \to \eta(\mathbf{r})$, and $3\epsilon(\mathbf{r})/(2\pi\rho_0 e^2 a^2) \to \epsilon(\mathbf{r})$, the SCF equations can then be written as

$$\omega_P(\mathbf{r}) = \chi_{PS}N\phi_S(\mathbf{r}) + \sum_{P'\neq P} \chi_{PP'}N\phi_{P'}(\mathbf{r}) + \eta(\mathbf{r}) \quad (10)$$

$$\omega_S(\mathbf{r}) = \sum_P \chi_{PS}N\phi_P(\mathbf{r}) + \eta(\mathbf{r}) \quad (11)$$

$$\omega_\pm(\mathbf{r}) = Nv_\pm\psi(\mathbf{r}) \quad (12)$$

$$\phi_P(\mathbf{r}) = \frac{\bar{\phi}_P N}{Q_P N_P}\int_0^{N_P/N} ds q_P(\mathbf{r}, s) q_P\left(\mathbf{r}, \frac{N_P}{N} - s\right) \quad (13)$$

$$\phi_M(\mathbf{r}) = \frac{\bar{\phi}_M}{Q_M}\exp\left[-\frac{\omega_M(\mathbf{r})}{N}\right] \quad (14)$$

$$-\sum_P \phi_P(\mathbf{r})\frac{dg_P(\mathbf{r})}{d\psi(\mathbf{r})} + v_+\phi_+(\mathbf{r}) + v_-\phi_-(\mathbf{r}) + \frac{1}{N}[\epsilon(\mathbf{r})\nabla^2\psi(\mathbf{r}) + \nabla\epsilon(\mathbf{r})\cdot\nabla\psi(\mathbf{r})] = 0 \quad (15)$$

$$\sum_P \phi_P(\mathbf{r}) + \phi_S(\mathbf{r}) - 1 = 0 \quad (16)$$

where $q_P(\mathbf{r},s)$ corresponds to the probability of finding the end-segment of a P polymer of length sN at $\mathbf{r}$, and it satisfies the modified diffusion equation

$$\frac{\partial q_P}{\partial s} = \nabla^2 q_P - [\omega_P(\mathbf{r}) - Ng_P(\mathbf{r})]q_P \quad (17)$$

with the initial condition $q_P(\mathbf{r}, 0) = 1$; and where $Q_P = (1/V)\int d\mathbf{r} q_P(\mathbf{r}, N_P/N)$ and $Q_M = (1/V)\int d\mathbf{r} \exp[-\omega_M(\mathbf{r})/N]$. The mean-field free energy per chain of length N is

$$f_c \equiv \frac{N\mathcal{F}}{\rho_0 V R_g^d} = \frac{1}{V}\int d\mathbf{r}\left\{\sum_P \left[\chi_{PS}N\phi_S(\mathbf{r}) + \frac{1}{2}\sum_{P'\neq P}\chi_{PP'}N\phi_{P'}(\mathbf{r}) - \omega_P(\mathbf{r})\right]\phi_P(\mathbf{r}) - \omega_S(\mathbf{r})\phi_S(\mathbf{r}) - \frac{\epsilon(\mathbf{r})}{2}|\nabla\psi(\mathbf{r})|^2\right\} - N\left(\sum_P \frac{\bar{\phi}_P}{N_P}\ln\frac{Q_P}{\bar{\phi}_P} + \sum_M \bar{\phi}_M \ln\frac{Q_M}{\bar{\phi}_M}\right) \quad (18)$$

Finally, we apply the incompressibility and the charge neutrality constraints on the whole system, which give

$$\bar{\phi}_S = 1 - \sum_P \bar{\phi}_P$$

$$\bar{\phi}_- = -\frac{1}{v_-}(v_+\bar{\phi}_+ + \sum_P v_P\alpha_P\bar{\phi}_P)$$

Assuming that one salt molecule generates one cation, we have $\bar{\phi}_+ = c_s - (\sum_{P\in\{v_P<0\}} v_P\alpha_P\bar{\phi}_P)/v_+$, where c_s denotes the salt

concentration (in units of ρ_0), and the summation is over the chain types that carry negative charges. Also, in the Poisson−Boltzmann equation, eq 15, we use the following linear approximation for the position-dependent dielectric constant:

$$\epsilon(\mathbf{r}) = \sum_{\mathrm{P}} \epsilon_{\mathrm{P}}\phi_{\mathrm{P}}(\mathbf{r}) + \epsilon_{\mathrm{S}}\phi_{\mathrm{S}}(\mathbf{r})$$

where ϵ_{P} and ϵ_{S} are the normalized dielectric constant of the P polymer and the solvent, respectively.

We solve the SCF equations in real space. The space domain is discretized (uniformly) at m nodes, denoted by $\mathbf{r}_i (i = 1,..., m)$. Representing the values of any field $p(\mathbf{r})$ at these nodes by a vector $\mathbf{p} \equiv [p(\mathbf{r}_1), p(\mathbf{r}_2),..., p(\mathbf{r}_m)]^T$, we choose $\boldsymbol{\omega}_{\mathrm{P}}$ and $\boldsymbol{\psi}$ as independent variables and reduce the SCF equations into a set of nonlinear equations $F_k = 0$ $(k = 1,...,(m_{\mathrm{P}} + 1)m)$, where m_{P} denotes the total number of chain types.[41] A quasi-Newton method[42] is used to solve these equations. Due to the computational expense associated with inversion of the Jacobian matrix $\partial\{F_k\}/\partial\{\boldsymbol{\omega}_{\mathrm{P}}, \boldsymbol{\psi}\}$ (which scales with m^3), this method limits our calculations to one-dimension in practice. It, however, provides fast convergence and high accuracy. In this work, the residual error $\sum_{k=1}^{(m_{\mathrm{P}}+1)m}|F_k|/[(m_{\mathrm{P}} + 1)m]$ is typically less than 10^{-12}.

We solve the modified diffusion equation, eq 17, by a pseudo-spectral method,[43] where fast Fourier transforms are performed using the software package developed at MIT.[44] (Depending on the boundary conditions, fast cosine or sine transforms may be used instead.[45]) Consistent with the $O((\Delta s)^3)$ error of this method (where Δs denotes the step size in the temporal (s) domain),[43] a composite Simpson's rule is used for the integrals in eq 13 as well as in the calculations of Q_{M} and f_c. Also, the spatial derivatives in eq 15 and in the calculation of f_c are approximated by the second-order central differences. In this paper, the numbers of grid points m and $n \equiv 1/\Delta s$ are chosen such that the accuracy of f_c is within $\pm 10^{-4}$; this typically requires m and n be on the order of 10^2 to 10^3.

Finally, it is worth noting that, with $\{\boldsymbol{\omega}_{\mathrm{P}}^*, \boldsymbol{\psi}^*\}$ being a solution to the SCF equations and c_1 and c_2 being arbitrary constants, if *all* the charge distributions are smeared, then $\{\boldsymbol{\omega}_{\mathrm{P}}^* + c_1, \boldsymbol{\psi}^* + c_2\}$ is also a solution; if any charge distribution is annealed, then $\{\boldsymbol{\omega}_{\mathrm{P}}^* + c_1, \boldsymbol{\psi}^*\}$ is also a solution. In both cases, these uniform shifts result in the same densities and the same free energy. We therefore set, for example, $Q_{\mathrm{A}} = \bar{\phi}_{\mathrm{A}}$ to obtain unique $\boldsymbol{\omega}_{\mathrm{P}}$; when *all* the charge distributions are smeared, we also set, say, $Q_+ = \bar{\phi}_+ > 0$ to obtain unique $\boldsymbol{\psi}$.

2.2. Charged Block Copolymers in Solution. It is straightforward to generalize the above formalism to charged block copolymer solutions. Here we consider the case of A−B diblock polyelectrolytes of chain length N. The average copolymer segmental density is denoted by $\bar{\phi}_{\mathrm{C}} \equiv n_{\mathrm{C}}N/(\rho_0 V)$, where n_{C} is the number of copolymer chains in the system. The volume fraction of the A block in the copolymer is denoted by f_{A}, and thus $\bar{\phi}_{\mathrm{A}} = f_{\mathrm{A}}\bar{\phi}_{\mathrm{C}}$ and $\bar{\phi}_{\mathrm{B}} = (1 - f_{\mathrm{A}})\bar{\phi}_{\mathrm{C}}$. The variable s along the chain contour is defined such that $s \in [0, f_{\mathrm{A}}N]$ corresponds to the A block and $s \in [f_{\mathrm{A}}N, N]$ to the B block; the limits of the above integrals over s are therefore changed correspondingly. Moreover, instead of eq 9, we now use the following single-chain partition function:

$$Q_{\mathrm{C}} \equiv \frac{1}{\mathscr{S}}\int \mathscr{D}\mathbf{R}\, \exp\left\{-\int_0^{f_{\mathrm{A}}N} \mathrm{d}s\left[\frac{3}{2a^2}(\dot{\mathbf{R}}(s))^2 + \omega_{\mathrm{A}}(\mathbf{R}(s)) - g_{\mathrm{A}}(\mathbf{R}(s))\right] - \int_{f_{\mathrm{A}}N}^{N} \mathrm{d}s\left[\frac{3}{2a^2}(\dot{\mathbf{R}}(s))^2 + \omega_{\mathrm{B}}(\mathbf{R}(s)) - g_{\mathrm{B}}(\mathbf{R}(s))\right]\right\} \quad (19)$$

where

$$\mathscr{S} \equiv \int \mathscr{D}\mathbf{R}\, \exp\left\{-\int_0^N \mathrm{d}s \frac{3}{2a^2}(\dot{\mathbf{R}}(s))^2\right\}$$

After the rescaling, with P being A and B, the only difference in the SCF equations is that eq 13 now becomes

$$\phi_{\mathrm{A}}(\mathbf{r}) = \frac{\bar{\phi}_{\mathrm{C}}}{Q_{\mathrm{C}}}\int_0^{f_{\mathrm{A}}} \mathrm{d}s q_{\mathrm{C}}(\mathbf{r}, s) q_{\mathrm{C}}^*(\mathbf{r}, 1 - s)$$

$$\phi_{\mathrm{B}}(\mathbf{r}) = \frac{\bar{\phi}_{\mathrm{C}}}{Q_{\mathrm{C}}}\int_{f_{\mathrm{A}}}^1 \mathrm{d}s q_{\mathrm{C}}(\mathbf{r}, s) q_{\mathrm{C}}^*(\mathbf{r}, 1 - s)$$

where $Q_{\mathrm{C}} = (1/V)\int \mathrm{d}\mathbf{r} q_{\mathrm{C}}(\mathbf{r}, 1)$, and $q_{\mathrm{C}}(\mathbf{r}, s)$ corresponds to the probability of finding a chain of length sN that starts from $s = 0$ (the A end) and ends at $\mathbf{r}$. Instead of eq 17, $q_{\mathrm{C}}(\mathbf{r}, s)$ satisfies the following modified diffusion equation:

$$\frac{\partial q_{\mathrm{C}}}{\partial s} = \begin{cases} \nabla^2 q_{\mathrm{C}} - [\omega_{\mathrm{A}}(\mathbf{r}) - Ng_{\mathrm{A}}(\mathbf{r})]q_{\mathrm{C}} & \text{if } s \le f_{\mathrm{A}} \\ \nabla^2 q_{\mathrm{C}} - [\omega_{\mathrm{B}}(\mathbf{r}) - Ng_{\mathrm{B}}(\mathbf{r})]q_{\mathrm{C}} & \text{if } s \ge f_{\mathrm{A}} \end{cases} \quad (20)$$

with the initial condition $q_{\mathrm{C}}(\mathbf{r}, 0) = 1$. By defining $t \equiv 1 - s$, a similar quantity $q_{\mathrm{C}}^*(\mathbf{r}, t)$ can be defined, which corresponds to the probability of finding a chain of length tN that starts from $t = 0$ (the B end) and ends at $\mathbf{r}$, and it satisfies

$$\frac{\partial q_{\mathrm{C}}^*}{\partial t} = \begin{cases} \nabla^2 q_{\mathrm{C}}^* - [\omega_{\mathrm{A}}(\mathbf{r}) - Ng_{\mathrm{A}}(\mathbf{r})]q_{\mathrm{C}}^* & \text{if } t \ge 1 - f_{\mathrm{A}} \\ \nabla^2 q_{\mathrm{C}}^* - [\omega_{\mathrm{B}}(\mathbf{r}) - Ng_{\mathrm{B}}(\mathbf{r})]q_{\mathrm{C}}^* & \text{if } t \le 1 - f_{\mathrm{A}} \end{cases} \quad (21)$$

with the initial condition $q_{\mathrm{C}}^*(\mathbf{r}, 0) = 1$. Finally, eq 18 becomes

$$f_c = \frac{1}{V}\int \mathrm{d}\mathbf{r}\Big[\chi_{\mathrm{AS}}N\phi_{\mathrm{A}}(\mathbf{r})\phi_{\mathrm{S}}(\mathbf{r}) + \chi_{\mathrm{BS}}N\phi_{\mathrm{B}}(\mathbf{r})\phi_{\mathrm{S}}(\mathbf{r}) + \chi_{\mathrm{AB}}N\phi_{\mathrm{A}}(\mathbf{r})\phi_{\mathrm{B}}(\mathbf{r}) - \omega_{\mathrm{A}}(\mathbf{r})\phi_{\mathrm{A}}(\mathbf{r}) - \omega_{\mathrm{B}}(\mathbf{r})\phi_{\mathrm{B}}(\mathbf{r}) - \omega_{\mathrm{S}}(\mathbf{r})\phi_{\mathrm{S}}(\mathbf{r}) - \frac{\epsilon(\mathbf{r})}{2}|\nabla\psi(\mathbf{r})|^2\Big] - \bar{\phi}_{\mathrm{C}}\ln\frac{Q_{\mathrm{C}}}{\bar{\phi}_{\mathrm{C}}} - N\sum_{\mathrm{M}}\bar{\phi}_{\mathrm{M}}\ln\frac{Q_{\mathrm{M}}}{\bar{\phi}_{\mathrm{M}}} \quad (22)$$

The SCF equations are solved accordingly, where we set $Q_{\mathrm{C}} = \bar{\phi}_{\mathrm{C}}$ to obtain unique $\boldsymbol{\omega}_{\mathrm{P}}$.

3. Results and Discussion

3.1. Interface of a Phase-Separated Polyelectrolyte Solution. Solutions of polyelectrolyte A in a poor solvent S can macroscopically phase separate into polymer-poor and polymer-rich phases under certain conditions. Here we apply the above SCF formalism to determine the one-dimensional density profiles across the (flat) interface between the two phases. This problem was briefly studied by Shi and Noolandi, who considered the case of the smeared charge distribution and the same dielectric constants of the polymer and the solvent (i.e., $\epsilon_{\mathrm{A}} = \epsilon_{\mathrm{S}}$).[14] Here we extend their study to cases of the annealed charge distribution and of different dielectric constants. As noted above, the dielectric constants of organic polymers (e.g., polystyrene) and polar solvents (e.g., water) could differ by 1 or 2 orders of magnitude. Our approach of solving the SCF equations is also different from the previous work, where the equilibrium bulk phases were used as reference states. That is, at a given $\bar{\phi}_{\mathrm{A}}$, Shi and Noolandi first solved the bulk

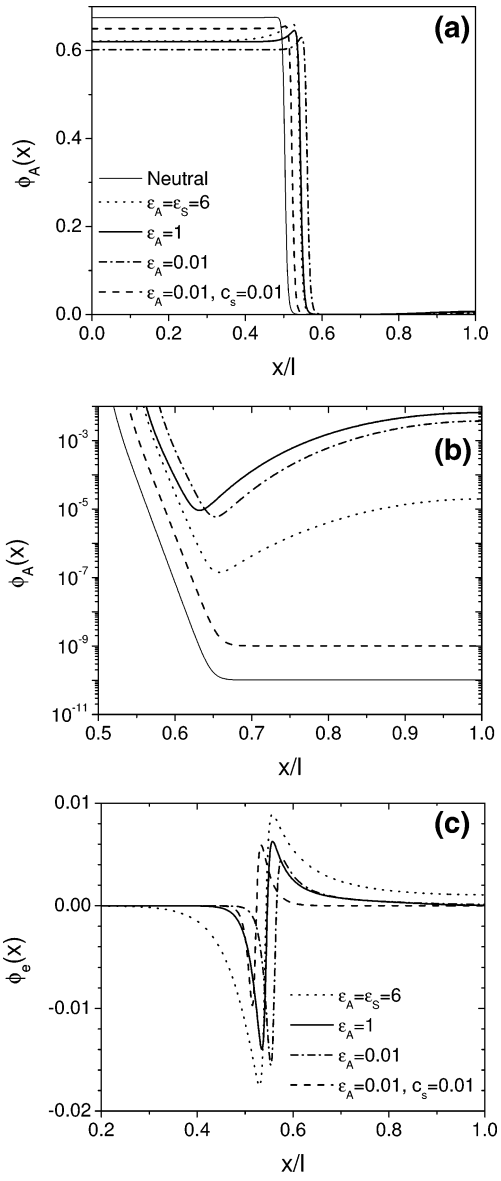

Figure 1. Density profiles of a phase-separated polyelectrolyte solution in the case of the smeared charged distribution, at $\epsilon_S = 1$ and $c_s = 0$ (unless otherwise specified). (a) Polymer density profiles across the interface between the polymer-rich and polymer-poor phases. (b) Semilogarithmic plot of the polymer density profiles in the polymer-poor phase, where the legend is the same as in (a). (c) Total charge density profiles.

equilibrium problem to determine the densities of the two phases, then imposed them as boundary conditions for solving the SCF equations;[14] we instead require that the first-order spatial derivatives be zero at the boundaries. This leads to some differences in the profiles, as shown below.

We set $N = 100$, $\alpha_A = 0.05$, $\chi_{AS} = 1$, $c_s = 0$ or 0.01, and solve the SCF equations in a one-dimensional cell of length $l \approx 29.394$ (in units of R_g); these parameters are the same as in ref 14. We also set $v_A = v_- = -v_+ = -1$ (which is just the opposite to ref 14), $\epsilon_S = 1$ (unless specified otherwise), and $\bar{\phi}_A = 0.34$. Figure 1 shows the polymer density profiles $\phi_A(x)$ and the total charge density profiles $\phi_e(x)$ for the smeared charge distribution, where x denotes the direction perpendicular to the interface. The case where the polymer is neutral is also shown in Figures 1a and 1b for comparison. We observe the same trends as reported in ref 14: (1) the charged polymer has larger miscibility with the poor solvent than the neutral polymer; (2) the charged polymer density profile is non-monotonic near the interface, as opposed to the neutral case; (3) added salt screens the electrostatic interactions, and thus reduces the miscibility and smooths the non-monotonic density profile; and (4) the total charge density profile exhibits a double-layer structure at the interface, and decays more rapidly into the polymer-rich phase than the polymer-poor phase.

Figure 1 also shows the effects of dielectric constants. If we take $a = 0.7$ nm and $\rho_0 = a^{-3}$, then $\epsilon_A = 0.01$ corresponds to a relative dielectric constant of about 1.68 at 25 °C. Note that the $\tau \equiv 4\pi\rho_0 a^2 e^2/(\epsilon k_B T) = 1$ case studied in ref 14 is equivalent to the $\epsilon_A = \epsilon_S = 6$ case here. Comparing it with the $\epsilon_A = 1$ case (where $\epsilon_S = 1$), we see that a larger dielectric constant leads to smaller miscibility of the polyelectrolyte with the solvent and longer decay length of the total charge density. The same trends, exhibited mainly for the polymer-rich phase, are observed by comparing the $\epsilon_A = 1$ case with the $\epsilon_A = 0.01$ case (where $\epsilon_S = 1$). Note that, in the $\epsilon_A = \epsilon_S = 6$ case, the decay length is so large that the bulk of the polymer-poor phase is apparently positively charged; this indicates that $l \approx 29.394$ is not enough to represent the whole interfacial region for such a large dielectric constant. Also, the shift of the interfacial position in Figures 1a and 1c is due to the fact that $\int dx\phi_A(x) = l\bar{\phi}_A$ in our calculations. In ref 14, $\phi_e = 0$ was imposed as boundary conditions and the interfacial position was fixed at $x = 0$.[46]

Figure 2 shows the density profiles for the annealed charge distribution. We see that both $\phi_A(x = 0)$ and $\phi_A(x = l)$ are larger than in the smeared case. Also, for the two salt-free cases, $\phi_A(x)$ in the polymer-poor phase exhibits behavior different than that in the corresponding smeared case. Finally, the decay length of the total charge density is shorter than in the smeared case. These are due to the characteristics of the annealed charge distribution, where the local segment dissociation is coupled to the electrostatic potential. Figure 3 shows the local degree of ionization $p_A(x) \equiv -dg_A(x)/(v_A d\psi(x))$ for the annealed case; we see that $p_A(x)$ is much larger than α_A in the polymer-poor phase.

The system studied here provides a simple example where the effects of various parameters in our theory can be examined. The RPA analysis described in the Appendix indicates that, in all the above cases, the homogeneous phase is unstable with respect to both the macroscopic phase separation and the microphase separation. We however do not pursue to determine which state is thermodynamically stable, due to the strong asymmetry of polyelectrolyte solutions; for such systems two- or three-dimensional structures may be competitive and thus three-dimensional calculations are required.

3.2. Symmetric Diblock Polyelectrolytes. As the second example, we study the microphase separation and the lamellar structure of symmetric diblock polyelectrolytes A−B (where the only difference between A and B is that they carry opposite charges) in a good solvent. In great contrast to their neutral counterparts, the ordered structures of block polyelectrolytes below the ODT have not been studied theoretically. Here we set $N_A = N_B = N/2 = 200$, $v_A = v_- = -v_B = -v_+ = -1$, $\alpha_A = \alpha_B = p$, and $\epsilon_A = \epsilon_B = \epsilon_P$. The two blocks have the same charge distribution (both are either smeared or annealed). To avoid the complication of possible macroscopic phase separation between the polymer and the solvent, we include a good, polar solvent in the system and set $\bar{\phi}_C = 0.8$, $\chi_{AS} = \chi_{BS} = 0$, and $\epsilon_S = 1$. For such a diblock polyelectrolyte solution, the A and B have an inherent symmetry, and the only possible microphase-separated structure is lamellae. In the following, we denote χ_{AB}

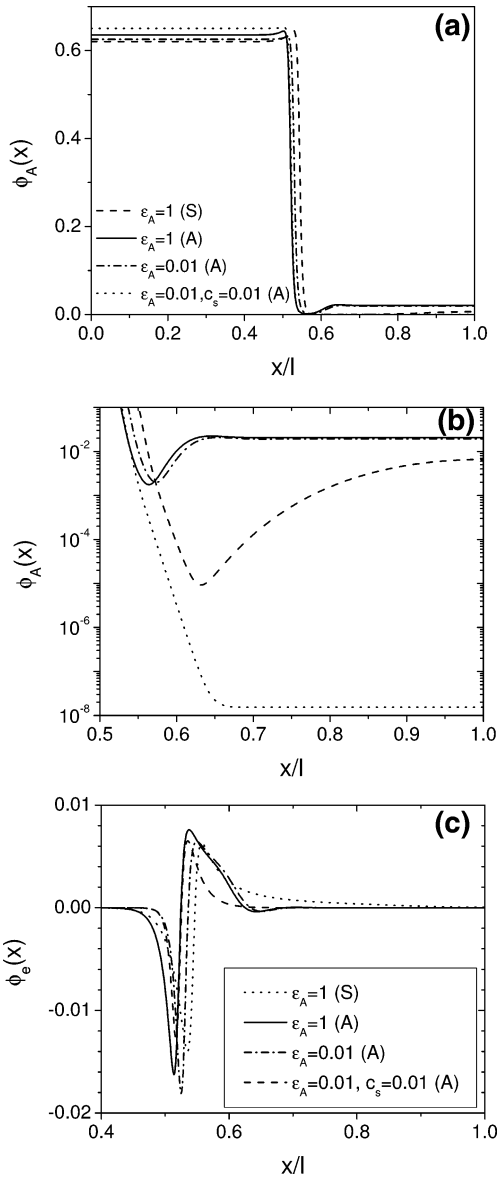

Figure 2. Density profiles of a phase-separated polyelectrolyte solution, at $\epsilon_S = 1$ and $c_s = 0$ (unless otherwise specified). The polymer has either the smeared charge distribution (denoted by "S" in the legend) or the annealed charge distribution (denoted by "A" in the legend). (a) Polymer density profiles across the interface between the polymer-rich and polymer-poor phases. (b) Semilogarithmic plot of the polymer density profiles in the polymer-poor phase, where the legend is the same as in (a). (c) Total charge density profiles.

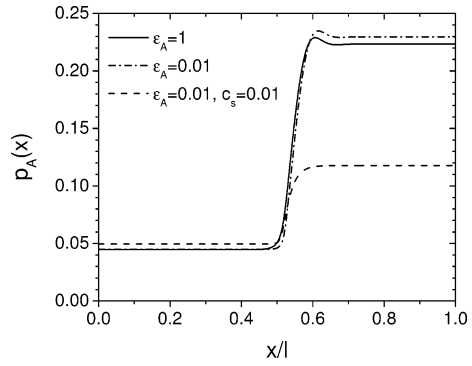

Figure 3. Local degree of dissociation of a phase-separated polyelectrolyte solution in the case of the annealed charge distribution, at $\epsilon_S = 1$ and $c_s = 0$ (unless otherwise specified).

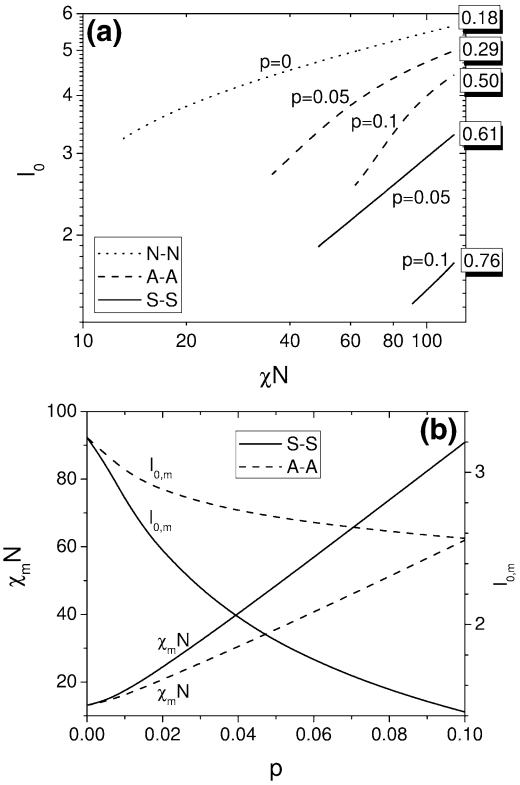

Figure 4. Results for symmetric diblock polyelectrolyte in a good solvent, at $\epsilon_A = \epsilon_B = \epsilon_S = 1$. In the legend, "N−N" denotes the case where both blocks are neutral (uncharged), "A−A" denotes the case where both blocks have the annealed charge distribution, and "S−S" denotes the case where both blocks have the smeared charge distribution. (a) log−log plot of equilibrium lamellar period as a function of χN, where the value of $\partial \ln l_0/\partial \ln(\chi N)$ at $\chi N = 120$ is given at the right end of each $l_0 \sim \chi N$ curve. (b) ODT properties as a function of p.

by χ and set $c_s = 0$, and examine the effects of different charge distributions and parameters (p, ϵ_P, and χN) on the ODT and on the lamellar structure of the system. The SCF equations are solved under periodic boundary conditions (PBC) in a one-dimensional unit cell that contains one period of lamellae; the unit cell length is adjusted to minimize f_c, and thus gives the bulk lamellar period l_0 (in units of R_g).

Figure 4a shows a log−log plot of l_0 as a function of χN, for the case of equal dielectric constants, i.e., $\epsilon_P = \epsilon_S = 1$. We see that l_0 increases with increasing χN and with decreasing p. It is of interest to examine the quantity $\gamma \equiv \partial \ln l_0/\partial \ln(\chi N)$; the value of γ at $\chi N = 120$ is given for each curve in the figure. For lamellae of neutral symmetric diblock copolymers, γ decreases monotonically from about 1/2 in the weak segregation limit to 1/6 in the strong segregation limit (recall that l_0 is in units of R_g).[9] From Figure 4a we see that γ decreases with increasing χN and with decreasing p.

At a given p, the left end of the $l_0 \sim \chi N$ curve in Figure 4a corresponds to the ODT. From Figure 4b we see that, at the ODT (denoted by the subscript "m"), $\chi_m N$ increases while $l_{0,m}$ decreases with increasing p. These ODT curves determined from the SCF calculations are in good agreement with the corresponding RPA results. The opposite charges on the copolymers therefore increase the compatibility of the two blocks. Figure 4 also indicates that the effects of charges in the annealed case are less pronounced than in the smeared case, both on the order−disorder transition and on the lamellar structure of the system.

Figure 5a shows the effects of p and dielectric constants on the equilibrium lamellar period, at $\chi N = 120$. We see that, for

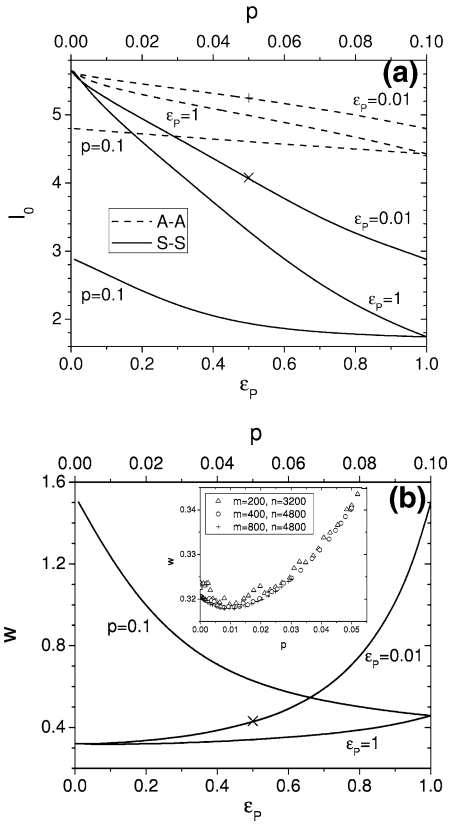

Figure 5. Effects of p and dielectric constants on the lamellae of symmetric diblock polyelectrolyte in a good solvent, at $\chi N = 120$ and $\epsilon_S = 1$. (a) Equilibrium lamellar period. Refer to Figure 4 for explanation of the legend. The value of l_0 calculated using $\epsilon_A = \epsilon_B = \epsilon_S = \bar{\epsilon} = 0.208$ and $p = 0.05$ is marked by the symbol $\times$ (for the smeared case) or $+$ (for the annealed case) in the plot. (b) A−B interfacial width calculated in the smeared case. The value of w calculated using $\epsilon_A = \epsilon_B = \epsilon_S = \bar{\epsilon} = 0.208$ and $p = 0.05$ is marked by the symbol $\times$ in the plot. The inset is for the $\epsilon_A = \epsilon_B = 1$ case.

all cases, l_0 decreases with increasing p and with increasing ϵ_P. Note, however, that the value of l_0 cannot be used as an indication for the segregation of the system; as shown below, larger l_0 does not necessarily correspond to stronger segregation. We therefore examine in Figure 5b the A−B interfacial width $w \equiv dx/d\phi_A$ (in units of R_g) at the A−B interface (defined by $\phi_A(x) = \phi_B(x)$), for the smeared charge distribution and at $\chi N = 120$. We see that w increases with increasing p, except in the range of p very close to 0. The inset of Figure 5b, which is for the $\epsilon_P = \epsilon_S = 1$ case, indicates a minimum of w around $p = 0.01$; it also shows that, due to the strong segregation of the system, large m and n are needed to calculate w with high accuracy. On the other hand, w decreases with increasing ϵ_P, which suggests that the segregation between A and B become stronger. Results for the annealed charge distribution and at $\chi N = 120$ (not shown) exhibit the same trends, with less pronounced effects.

Because the good solvent is almost uniformly distributed in the system, results of the $\epsilon_P = 0.01$ case (where $\epsilon_S = 1$) are very close to those of the $\epsilon_P = \epsilon_S = \bar{\epsilon} = 0.208$ case, where $\bar{\epsilon} \equiv \epsilon_A\bar{\phi}_A + \epsilon_B\bar{\phi}_B + \epsilon_S\bar{\phi}_S$; this is shown in Figure 5 for $p = 0.05$. Therefore, varying ϵ_P from 0.01 to 1 with $\epsilon_S = 1$ corresponds to varying $\epsilon_P = \epsilon_S = \bar{\epsilon}$ from 0.208 to 1. Figure 6a shows the effects of dielectric constants on the order parameter profile $\phi_A(x) - \phi_B(x)$ of the system at $\chi N = 120$ and $p = 0.1$. Consistent with the above results of A−B interfacial width, we see that increasing the dielectric constants results in stronger segregation between A and B, and that this effect is less pronounced in the annealed case than in the smeared case. Figure 6b shows the effects of dielectric constants on the total charge density profile of the system at $\chi N = 120$ and $p = 0.1$. An electric double-layer is seen at each A−B interface and has longer decay length with increasing dielectric constants. The decay length is also longer in the smeared case, where the two double-layers at adjacent interfaces interfere with each other, than in the annealed case. These observations are consistent with the above case of phase-separated polyelectrolyte solutions.

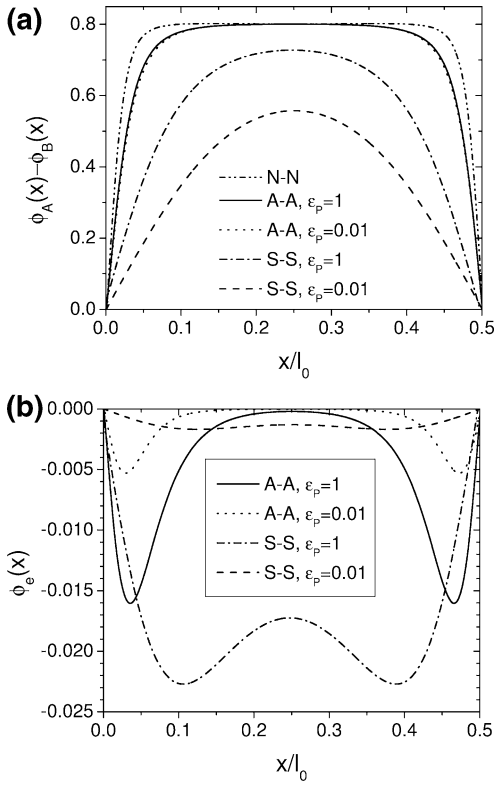

Figure 6. Lamellar profiles of symmetric diblock polyelectrolyte in a good solvent, at $\chi N = 120$, $p = 0.1$, and $\epsilon_S = 1$. Because of the symmetry between A and B, only the profiles in the A domain are shown. (a) Order parameter profiles. (b) Total charge density profiles. Refer to Figure 4 for explanation of the legend.

3.3. Polyelectrolyte Blends. Polyelectrolyte blends can have both macroscopic phase separation and microphase separation. As the third example, we study the lamellar structure and the competition between the macroscopic phase separation and the microphase separation of polyelectrolyte blends A/B with A and B having the same chain length. In the following, two systems are investigated: In the case of symmetric polyelectrolyte blends, we choose the system to be identical to the symmetric diblock polyeletrolytes studied above, apart from the covalent bond between the A and B blocks; our results therefore reveal the consequence of the covalent bond. Finally, we revisit the phase behavior of the blends of charged and neutral polymers A/B studied by Nyrkova et al.[35] and compare our results with theirs.

3.3.1. Symmetric Polyelectrolyte Blends. For symmetric polyelectrolyte blends A/B in a good solvent S, we set $N_A = N_B = N = 200$, $\bar{\phi}_A = \bar{\phi}_B = 0.4$, and $\chi_{AS} = \chi_{BS} = 0$. Both the A and B polymers have the smeared charge distribution, with $\upsilon_A = \upsilon_- = -\upsilon_B = -\upsilon_+ = -1$, $\alpha_A = \alpha_B = p$, and $\epsilon_A = \epsilon_B = \epsilon_P$. Again, in this case the A and B have an inherent symmetry, and the only possible microphase-separated structure is lamellae. In the following, we denote χ_{AB} by χ and set $c_s = 0$, and study the phase behavior of the symmetric polyelectrolyte blends. For macroscopic phase separation, we consider only the case where

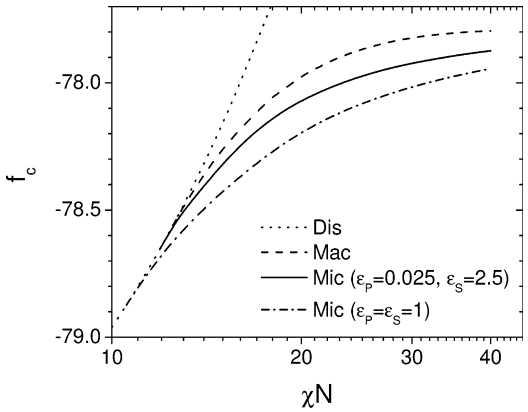

Figure 7. Semilogarithmic plot of the free energies of various phases for symmetric polyelectrolyte blends in a good solvent, at $p = 0.02$. In the legend, "Dis" denotes the disordered phase, "Mac" denotes the macroscopically phase-separated state, and "Mic" denotes the lamellae.

two homogeneous phases are at equilibrium. For microphase separation, the SCF equations are solved under PBC in a one-dimensional unit cell that contains one period of lamellae; the unit cell length is adjusted to minimize f_c, and thus gives the bulk lamellar period l_0 (in units of R_g).

Figure 7 compares the free energies of various phases as a function of χN, at $p = 0.02$. The disordered (homogeneous) phase always has the highest free energy over the range of χN in the figure. The free energy curve for macroscopic phase separation starts from the critical point (denoted by the subscript "c"), which is at $\chi_c N = 12.5$, and is below the curve for the disordered phase for $\chi N > \chi_c N$. The curve for microphase separation starts from the ODT, which is predicted by the SCF calculations to be at $\chi_m N \approx 10.54$ (with $l_{0,m} \approx 4.17$) for the $\epsilon_P = \epsilon_S = 1$ case and at $\chi_m N \approx 11.93$ (with $l_{0,m} \approx 4.94$) for the $\epsilon_P = 0.025$ and $\epsilon_S = 2.5$ case, respectively; these again are in good agreement with the RPA analysis (presented in Appendix A1) using $\bar{\epsilon} = 1$ and $\bar{\epsilon} = 0.52$, respectively. Figure 7 shows that in these two cases lamellae have the lowest free energy for $\chi N > \chi_m N$. The stability of the microphase-separated state over the macroscopically phase-separated state largely depends on the dielectric constants of the system. As shown in Appendix A3, lamellar structure cannot be obtained for small $\bar{\epsilon}$, e.g., in the case of $\epsilon_P = 0.01$ and $\epsilon_S = 1$.

Figure 8 shows the effects of various parameters (χN, p, and dielectric constants) on the lamellar structure of the system. As expected, l_0 increases with increasing χN and with decreasing p, while w exhibits the opposite trend (not shown); this is the same as in the case of symmetric diblock polyelectrolytes. However, the range of l_0 for polyelectrolyte blends is much larger than that of diblocks. Note that it is difficult to perform the SCF calculations for lamellae of large period and small interfacial width, which require large value of m to reach the given accuracy. In Figure 8a, the left end of each curve corresponds to the ODT. We see that, in contrast to the case of symmetric diblock polyelectrolytes, γ increases with increasing χN. At large χN, a power-law relationship between l_0 and χN is observed; the value of γ at $\chi N = 40$ is given for each curve in Figure 8a. In Figure 8b, the right end of each curve corresponds to the ODT, and l_0 diverges at $p = 0$. Figures 8c and 8d show the effects of dielectric constants, where we see that both l_0 and w decrease with increasing $\bar{\epsilon}$ (at a given χN and p); this is again the same as in the case of symmetric diblock polyelectrolytes. The results shown in Figures 8c and 8d are for $\epsilon_S = 2.5$; they virtually overlap with the results for $\epsilon_P = \epsilon_S = \bar{\epsilon}$ (not shown), due to the almost uniform distribution of the good solvent in the system.

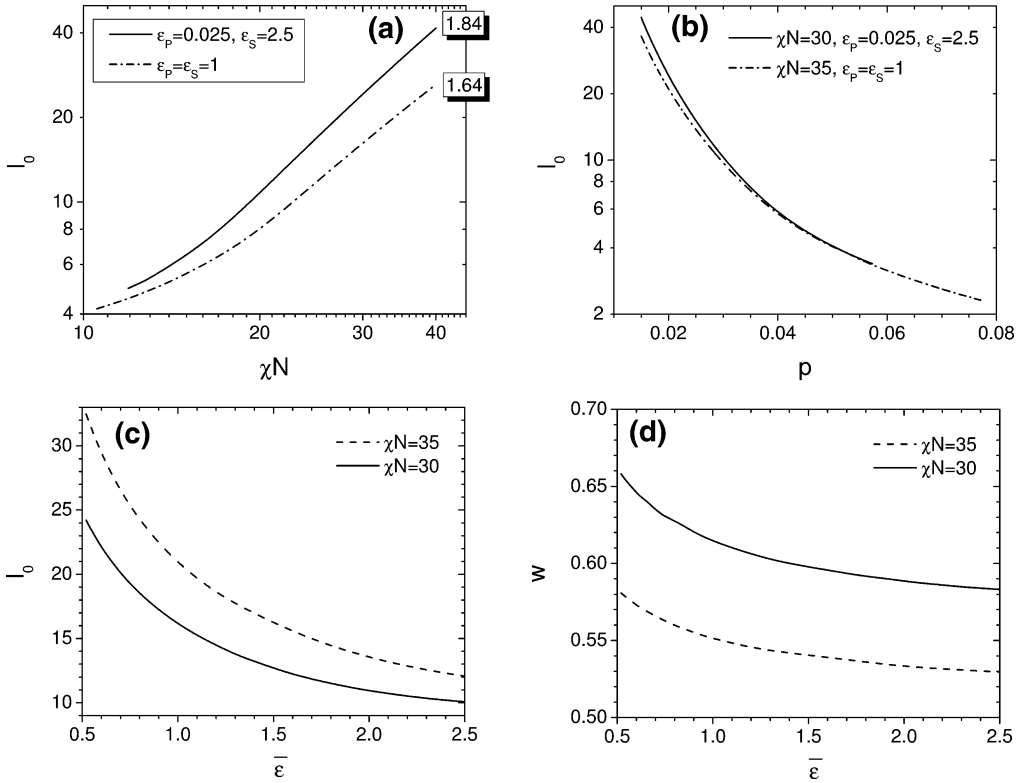

Figure 8. Effects of χN, p, and dielectric constants on the lamellae of symmetric polyelectrolyte blends in a good solvent. (a) log−log plot of equilibrium lamellar period as a function of χN, at $p = 0.02$. The value of $\partial \ln l_0 / \partial \ln(\chi N)$ at $\chi N = 40$ is given at the right end of each curve. (b) Semilogarithmic plot of equilibrium lamellar period as a function of p. (c) Equilibrium lamellar period as a function of dielectric constants, at $p = 0.02$ and $\epsilon_S = 2.5$. (d) Interfacial width as a function of dielectric constants, at $p = 0.02$ and $\epsilon_S = 2.5$.

Finally, using the RPA we can compare the ODT properties of the symmetric polyelectrolyte blends with those of the diblocks studied above. This is done in Appendix A2, where we also see that the effects of charges in the annealed case are less pronounced than in the smeared case.

3.3.2. Blends of Charged and Neutral Polymers. In this case the A polymers have the smeared charge distribution with $\upsilon_A = -\upsilon_+ = -1$ and $\alpha_A = 0.01$, and the B polymers are neutral. We set $N_A = N_B = N = 1000$, $\bar{\phi}_A = \bar{\phi}_B = 1/2$ (complete dissociation of polyelectrolyte segments is assumed although no solvent presents in the system), and $\epsilon_A = \epsilon_B = 2$. We again denote χ_{AB} by χ and set $c_s = 0$. This system is equivalent to the $\tau \equiv 4\pi e^2/(\epsilon k_B T a) = 3$ case studied by Nyrkova et al., who performed one-dimensional calculations to determine phase diagrams of the system of interest (in their work $\rho_0 = a^{-3}$).[35] Similar to the above case of symmetric blends, both macroscopic phase separation and microphase separation can occur under certain conditions. The phase diagram obtained by Nyrkova et al. was presented in Figure 6b of their paper; for $\bar{\phi}_A = 1/2$, microphase-separated state (lamellar structure) was shown to be stable in the range of $10 \lesssim \chi N \lesssim 17$, while the disordered and the macroscopically phase-separated states are stable for smaller and larger χN, respectively.[35]

However, the stability of the macroscopically phase-separated state (into two homogeneous phases) at large χN (i.e., at $\chi N \gtrsim 47$ as predicted in ref 35) is questionable. In the case of uniform dielectric constant, if we make the following two assumptions: (1) the free energy of the microphase-separated state monotonically increases with increasing period $l > l_0$ and (2) the macroscopically phase-separated state is equivalent to a microphase-separated state with an infinitely large period at the same χN, then the free energy curve for the macroscopically phase-separated state (as a function of χN) can never cross the free energy curve for the microphase-separated state having a *finite* l_0. Therefore, as long as l_0 does not diverge at any finite χN (note that a power-law relation between l_0 and χN is observed at large χN in our calculations), the macroscopically phase-separated state cannot become stable, as χN increases, over the microphase-separated state (which is stable at smaller χN). Furthermore, two factors limited the accuracy of the calculations by Nyrkova et al: (1) a square-gradient free-energy functional was used in their calculations, which is not uniformly valid at arbitrary χN,[36] and (2) a small number of grids in real space, namely $m = 50$, was used in their calculations. This is not enough for calculations at large χN, where lamellae have large period and small interfacial width. We therefore revisit the phase diagram of this system using the SCF calculations.

Figure 9 compares the free energies of various phases as a function of χN. We see that the lamellar phase is stable for $\chi N > \chi_m N \approx 8.93$, while the disordered phase is stable for smaller χN. The curve for macroscopic phase separation (into two homogeneous phases) starts from $\chi N \approx 10.33$ and is between those for the disordered phase and for the lamellae (within the range of our calculation). The difference of f_c between the macroscopically phase-separated and the microphase-separated states exhibits a maximum around $\chi N \approx 21.6$.

Finally, it is worth noting that, due to the broken symmetry between the A and B polymers, the critical point for the macroscopic phase separation is at $\chi_c N \approx 9.3166$ (with $\phi_{A,c} \approx 0.7683$). The asymmetry of the microphase-separated structure, however, is much less significant; $0.496 < l_A/l_0 < 1/2$ within the range of our one-dimensional calculations, where l_A denotes the length of the A domain (in units of R_g). The formation of lamellae as the microphase-separated structure is therefore justified. Furthermore, to determine the complete phase diagram of the system, the possibility of the macroscopic phase separation where at least one of the phases has a microphase-separated structure needs to be considered; this is beyond the scope of the current paper.

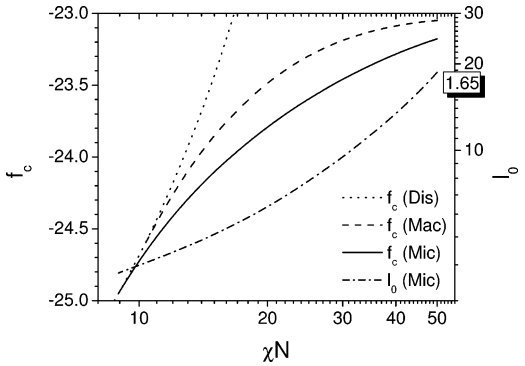

Figure 9. Semilogarithmic plot of the free energies of various phases for blends of charged and neutral polymers. The lamellar period of the microphase-separated state is also shown on a log−log plot, where the value of $\partial \ln l_0/\partial \ln(\chi N)$ at $\chi N = 50$ is given at the right end of the curve. Refer to Figure 7 for explanation of the legend.

4. Summary and Conclusions

In this work, a self-consistent field theory is applied to inhomogeneous polyelectrolyte systems. Both the smeared and the annealed charge distributions are considered, corresponding to strongly and weakly dissociating polymers, respectively. The modified diffusion equation describing the chain conformations is solved by a recently proposed pseudo-spectral method.[43] The electrostatic interactions are described by the Poisson−Boltzmann equation, where the dielectric constant of the system is treated as position-dependent to take into account the large dielectric difference between hydrophobic polymers and water-like solvents. The self-consistent mean-field equations obtained under the saddle-point approximation are solved in real space by a quasi-Newton method,[42] which leads to fast convergence and high accuracy but limits our calculations to one dimension.

To understand the effects of various parameters in our theory, we first studied the interface of a phase-separated polyelectrolyte solution in a poor solvent. We found that the charged polymer has larger miscibility with the poor solvent than the neutral polymer. This effect is reduced by the added salt, which screens the electrostatic interactions. The total charge density profile exhibits a double-layer structure at the interface, and the polymer-rich phase has a shorter decay length than the polymer-poor phase. We also found that a larger dielectric constant leads to smaller miscibility of the polyelectrolyte with the solvent and longer decay length of the total charge density. Differences between the smeared and the annealed charge distributions are also revealed.

We next investigated the order−disorder transition (ODT) and the lamellar structure of symmetric diblock polyelectrolytes A−B in a good solvent (where the only difference between A and B is that they carry opposite charges). We found that the opposite charges increase the compatibility of the two blocks and decrease the bulk lamellar period l_0 (in units of the radius of gyration of the chain). Larger dielectric constants result in stronger segregation between A and B, while decreasing l_0. Similar to the previous case, an electric double-layer was found at each A−B interface and has longer decay length with increasing dielectric constants. These effects are less pronounced in the annealed case than in the smeared case.

The phase behavior of polyelectrolyte blends, which can exhibit both macroscopic phase separation and microphase separation, was also examined. The order−disorder transition and the lamellar structure of symmetric polyelectrolyte blends A/B, which are identical to the above symmetric diblock polyelectrolytes apart from the A−B covalent bond, exhibit behavior similar to the diblocks. Due to the A−B covalent bond, however, there are some differences between the two systems: (1) the range of l_0 for blends is much larger than that of diblocks, and (2) $\partial \ln l_0/\partial \ln(\chi N)$ increases with increasing χN for blends and decreases for diblocks. As degrees of ionization α_P increase, the influence of the covalent bond becomes weaker compared to the electrostatic interactions; the differences between the two systems are therefore smaller. For polyelectrolyte blends, larger dielectric constants of the system stabilize the microphase-separated state over the macroscopically phase-separated state. It is unlikely that, by increasing χN, the microphase-separated state can give way at *finite* χN to the macroscopically phase-separated state where two homogeneous phases are at equilibrium (which can be viewed as the former state with infinitely large l_0), as long as l_0 does not diverge at any finite χN (a power-law relationship between l_0 and χN is observed at large χN).

All the calculations presented in this paper are one-dimensional; two- and three-dimensional calculations are necessary to explore ordered structures other than lamellae. In addition, the theory presented here can be applied only to weakly charged polyelectrolytes (e.g., $\alpha_P \lesssim 0.1$), where the chains remain flexible and their conformations can be described by the Gaussian chain model, eq 2. For strongly charged polyelectrolytes, chain-stretching due to repulsion between adjacent charged segments needs to be properly taken into account; models with finite extensibility of bonds can therefore be used in this context to replace eq 2. Furthermore, to relax the mean-field approximation, field-theoretic simulations of polyelectrolyte systems that allow the sampling of fluctuations are certainly of interest. Work along these directions is undergoing and will be the subject of future publications.

Acknowledgment. This work was partially supported by the University of California−Los Alamos National Laboratory CARE program and by the MRSEC program of the National Science Foundation under Award No. DMR00-80034. Use of the MRL central computing facilities is also gratefully acknowledged.

5. Appendix: Random Phase Approximation

A1. General Results. Here we derive the RPA results from our theory for both the smeared and the annealed charge distributions, following the derivation of Shi and Noolandi.[14] As in section 2, we start with charged homopolymer solutions. We perturb the fields around their value in the homogeneous phase

$$\phi_j(\mathbf{r}) = \bar{\phi}_j + \delta\phi_j(\mathbf{r})$$
$$\omega_j(\mathbf{r}) = \bar{\omega}_j + \delta\omega_j(\mathbf{r})$$
$$\psi(\mathbf{r}) = \bar{\psi} + \delta\psi(\mathbf{r})$$

and set $\bar{\omega}_j = 0$ and $\bar{\psi} = 0$ without loss of generality. We also define $\omega_P^{\text{eff}}(\mathbf{r}) \equiv \omega_P(\mathbf{r}) - Ng_P(\mathbf{r})$ in accordance with eq 17. For the smeared charge distribution

$$\delta\omega_P^{\text{eff}}(\mathbf{r}) = \delta\omega_P(\mathbf{r}) + \alpha_P N v_P \delta\psi(\mathbf{r})$$

while for the annealed charge distribution $\delta\omega_P^{\text{eff}}(\mathbf{r})$ can be expanded to the second order as

$$\delta\omega_P^{\text{eff}}(\mathbf{r}) \approx \delta\omega_P(\mathbf{r}) + \alpha_P N v_P \delta\psi(\mathbf{r}) - \frac{\alpha_P(1-\alpha_P)}{2} N v_P^2 (\delta\psi(\mathbf{r}))^2$$

The single-chain partition function is then approximated to the second order as

$$Q_P \approx \bar{Q}_P \exp\left[-\frac{N_P}{VN}\delta\hat{\omega}_P^{\text{eff}}(\mathbf{0}) + \frac{{N_P}^2}{2VN^2}\int \frac{d\mathbf{k}}{(2\pi)^3} P_P\left(k^2\frac{R_{g,P}^2}{R_g^2}\right)\delta\hat{\omega}_P^{\text{eff}}(\mathbf{k})\delta\hat{\omega}_P^{\text{eff}}(-\mathbf{k})\right]$$

where $\delta\hat{\omega}_P^{\text{eff}}(\mathbf{k})$ is the Fourier transform of $\delta\omega_P^{\text{eff}}(\mathbf{r})$, i.e., $\delta\hat{\omega}_P^{\text{eff}}(\mathbf{k}) \equiv \int d\mathbf{r} e^{-i\mathbf{k}\cdot\mathbf{r}}\, \delta\omega_P^{\text{eff}}(\mathbf{r})$; $P_P(k^2R_{g,P}^2/R_g^2)$ is the form factor of the P polymer, which for Gaussian chains can be described by the Debye function, i.e., $P_P(x) = 2(e^{-x} + x - 1)/x^2$, where $x \equiv k^2R_{g,P}^2/R_g^2$ and $R_{g,P} \equiv a\sqrt{N_P/6}$; and recall that $\mathbf{r}$ is in units of R_g. Similarly,

$$Q_M \approx \bar{Q}_M \exp\left[-\frac{1}{VN}\delta\hat{\omega}_M(\mathbf{0}) + \frac{1}{2VN^2}\int \frac{d\mathbf{k}}{(2\pi)^3}\delta\hat{\omega}_M(\mathbf{k})\delta\hat{\omega}_M(-\mathbf{k})\right]$$

Inserting the above equations into the following expression of the free energy per chain corresponding to eq 8, where $\eta(\mathbf{r})$ is eliminated by the incompressibility,

$$f_c = \frac{1}{V}\int d\mathbf{r}\left\{\sum_P\left[\frac{1}{2}\sum_{P'\neq P}\chi_{PP'}N\phi_{P'}(\mathbf{r}) + \chi_{PS}N\phi_S(\mathbf{r}) - \omega_P(\mathbf{r})\right]\phi_P(\mathbf{r}) - \omega_S(\mathbf{r})\phi_S(\mathbf{r}) + [v_+N\psi(\mathbf{r}) - \omega_+(\mathbf{r})]\phi_+(\mathbf{r}) + [v_-N\psi(\mathbf{r}) - \omega_-(\mathbf{r})]\phi_-(\mathbf{r}) - \frac{\epsilon(\mathbf{r})}{2}|\nabla\psi(\mathbf{r})|^2\right\} - N\left(\sum_P \frac{\bar{\phi}_P}{N_P}\ln\frac{Q_P}{\bar{\phi}_P} + \sum_M \bar{\phi}_M \ln\frac{Q_M}{\bar{\phi}_M}\right) \quad (23)$$

and noting that $\int d\mathbf{r}\delta\phi_j(\mathbf{r}) = 0$, $\int d\mathbf{r}\delta\omega_j(\mathbf{r}) = 0$, and $\int d\mathbf{r}\delta\psi(\mathbf{r}) = 0$, we obtain $f_c = \bar{f}_c + f_c^{(1)} + f_c^{(2)}$, where the first-order term $f_c^{(1)} = 0$, and the second-order term can be written as

$$f_c^{(2)} = \frac{1}{V}\int \frac{d\mathbf{k}}{(2\pi)^3}\left\{\frac{1}{2}\sum_{P,P'\neq P}\chi_{PP'}N\delta\hat{\phi}_P(\mathbf{k})\delta\hat{\phi}_{P'}(-\mathbf{k}) + \sum_P\chi_{PS}N\delta\hat{\phi}_P(\mathbf{k})\delta\hat{\phi}_S(-\mathbf{k}) - \sum_P\delta\hat{\omega}_P(\mathbf{k})\left[\delta\hat{\phi}_P(-\mathbf{k}) + \bar{\phi}_P N_P P_P(x)\left(\frac{1}{2N}\delta\hat{\omega}_P(-\mathbf{k}) + \alpha_P v_P\delta\hat{\psi}(-\mathbf{k})\right)\right] - \sum_M\left[\delta\hat{\omega}_M(\mathbf{k})\delta\hat{\phi}_M(-\mathbf{k}) + \frac{\bar{\phi}_M}{2N}\delta\hat{\omega}_M(\mathbf{k})\delta\hat{\omega}_M(-\mathbf{k})\right] + N[v_+\delta\hat{\phi}_+(\mathbf{k}) + v_-\delta\hat{\phi}_-(\mathbf{k})]\delta\hat{\psi}(-\mathbf{k}) - \frac{1}{2}[D(k) + \sum_P\bar{\phi}_P N_P P_P(x)N{\alpha_P}^2{v_P}^2]\delta\hat{\psi}(\mathbf{k})\delta\hat{\psi}(-\mathbf{k})\right\} \quad (24)$$

where $\underline{D}(k) \equiv \bar{\epsilon}k^2 + \sum_{P\in\{\text{annealed}\}}\alpha_P(1-\alpha_P)Nv_P^2\bar{\phi}_P$ in which $\bar{\epsilon} \equiv \sum_{P\epsilon P}\bar{\phi}_P + \epsilon_S\bar{\phi}_S$, and in which the summation is over the chain types that have the annealed charge distribution. By setting $\delta f_c^{(2)}/\delta\delta\hat{\omega}_j(\mathbf{k}) = 0$ and $\delta f_c^{(2)}/\delta\delta\hat{\psi}(\mathbf{k}) = 0$, we obtain

$$\delta\hat{\omega}_P(\mathbf{k}) = -\frac{N}{\bar{\phi}_P N_P P_P(x)}\delta\hat{\phi}_P(\mathbf{k}) - N\alpha_P v_P\delta\hat{\psi}(\mathbf{k}) \quad (25)$$

$$\delta\hat{\omega}_M(\mathbf{k}) = -\frac{N}{\bar{\phi}_M}\delta\hat{\phi}_M(\mathbf{k}) \quad (26)$$

$$\delta\hat{\psi}(\mathbf{k}) = \frac{N}{D(k)}\delta\hat{\phi}_e^S(\mathbf{k}) \quad (27)$$

where $\delta\hat{\phi}_e^S(\mathbf{k}) \equiv \sum_P\alpha_P v_P\delta\hat{\phi}_P(\mathbf{k}) + v_+\delta\hat{\phi}_+(\mathbf{k}) + v_-\delta\hat{\phi}_-(\mathbf{k})$ corresponds to the total charge density variation when all the polymers have the smeared charge distribution. As in ref 14, by substituting eqs 25−27 into eq 24 and then setting $\delta f_c^{(2)}/\delta\delta\hat{\phi}_\pm(\mathbf{k}) = 0$, we have

$$\delta\hat{\phi}_\pm(\mathbf{k}) = -\frac{\bar{\phi}_\pm Nv_\pm}{D(k)}\delta\hat{\phi}_e^S(\mathbf{k})$$

Noting from the incompressibility that $\delta\hat{\phi}_S(\mathbf{k}) = -\sum_P\delta\hat{\phi}_P(\mathbf{k})$, $f_c^{(2)}$ can finally be written as

$$f_c^{(2)} = \frac{N}{2V}\int\frac{d\mathbf{k}}{(2\pi)^3}\sum_{P,P'}\left(\chi_{PP'} - \chi_{PS} - \chi_{P'S} + \frac{1}{\bar{\phi}_S} + \frac{v_P v_{P'}\alpha_P\alpha_{P'}}{D(k)/N + \kappa^2}\right)\delta\hat{\phi}_P(\mathbf{k})\delta\hat{\phi}_{P'}(-\mathbf{k}) + \sum_P\frac{1}{\bar{\phi}_P N_P P_P(x)}\delta\hat{\phi}_P(\mathbf{k})\delta\hat{\phi}_P(-\mathbf{k}) \quad (28)$$

where $\chi_{PP} = 0$, and $\kappa^2 \equiv v_+^2\bar{\phi}_+ + v_-^2\bar{\phi}_-$ gives the Debye−Hückel screening length κ^{-1}. The structure matrix $\mathbf{S}(k)$ can therefore be written as

$$\mathbf{S}^{-1}(k) = \mathbf{S}_0{}^{-1}(k) + \boldsymbol{\theta} + \alpha(k)\mathbf{F}$$

where

$$S_{0,PP'}(k) = \begin{cases}\bar{\phi}_P N_P P_P(x) & \text{if } P{=}P'\\ 0 & \text{if } P{\neq}P'\end{cases} \quad (29)$$

$$\theta_{PP'} = \chi_{PP'} - \chi_{PS} - \chi_{P'S} + 1/\bar{\phi}_S$$

$$\alpha(k) \equiv \frac{1}{D(k)/N + \kappa^2}$$

$$F_{PP'} = v_P v_{P'}\alpha_P\alpha_{P'}$$

The above RPA results can be generalized to charged block copolymer solutions. For the case of A−B diblock polyelectrolytes of chain length N, with P and P′ being A and B, the only difference is that eq 29 now becomes[32]

$$\mathbf{S}_0(k) = \bar{\phi}_C N\begin{bmatrix} P(f_A,x) & \frac{P(1,x) - P(f_A,x) - P(1-f_A,x)}{2}\\ \frac{P(1,x) - P(f_A,x) - P(1-f_A,x)}{2} & P(1-f_A,x)\end{bmatrix}$$

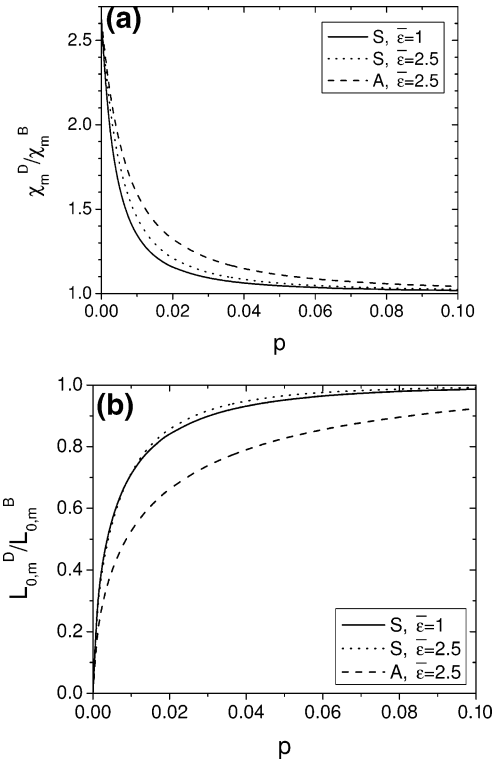

Figure 10. Comparison of the ODT properties of symmetric diblock polyelectrolytes A−B (denoted by the superscript "D") with those of corresponding blends A/B (denoted by the superscript "B"), using the RPA. In the legend, "S" denotes the case where both the A and B have the smeared charge distribution, and "A" denotes the case where both the A and B have the annealed charge distribution.

where $\bar{\phi}_C$ denotes the copolymer segmental density, $P(f, x) \equiv 2[fx + \exp(-fx) - 1]/x^2$, and $x = k^2$.

A2. Comparison of ODT Properties of Symmetric Diblock Polyelectrolytes and Corresponding Blends. The system of symmetric polyelectrolyte blends studied in section 3.3.1 can be viewed as identical to that of symmetric diblock polyeletrolytes studied in section 3.2, apart from the covalent bond between the A and B blocks. Here we compare the ODT properties of these two systems using the RPA results described above; the results are shown in Figure 10. At $p = 0$, the ratio of χ_m of the diblocks (denoted by the superscript "D") over that of the blends (denoted by the superscript "B"), which is effectively the critical point for macroscopic phase separation, is approximately 2.624. As expected, as p increases, the influence of the covalent bond becomes weaker compared to the electrostatic interactions; the differences between the two systems are therefore smaller, and both χ_m^D/χ_m^B and $L_{0,m}^D/L_{0,m}^B$ go to 1, where $L_0 \equiv l_0R_g$. Figure 10 also shows that the effects of charges in the annealed case are less pronounced than in the smeared case. The RPA analysis indicates that, at $\bar{\epsilon} = 1$, the symmetric polyelectrolyte blends cannot have microphase separation in the annealed case, unless $p \gtrsim 0.0636$.

A3. Simplified Results for Symmetric Polyelectrolyte Blends. For symmetric polyelectrolyte blends A/B in a solvent S, we have $N_A = N_B = N$,$P_A(x) = P_B(x) = P(k^2)$, $\bar{\phi}_A = \bar{\phi}_B = \phi/2$, and $\chi_{AS} = \chi_{BS} = \chi_{PS}$. We denote χ_{AB} by χ. The A and B polymers have the same charge distribution (both are either smeared or annealed), and we set $v_A = v_- = -v_B = -v_+ = -1$ and $\alpha_A = \alpha_B = p$. For symmetric systems, the RPA results of microphase separation give the order−disorder transition temperature χ_m and the corresponding lamellar period $2\pi/k_m$. In this case, the structure factor of the system can be written

as[30]

$$S_{AA}(k) = \phi NP(k^2)\Big[2 + \phi NP(k^2)\Big(\frac{1}{1-\phi} - 2\chi_{PS} + \alpha(k)p^2\Big)\Big] \Big/ \Big\{\Big[2 + \phi NP(k^2)\Big(\frac{1}{1-\phi} - 2\chi_{PS} + \alpha(k)p^2\Big)\Big]^2 - \Big[\phi NP(k^2)\Big(\frac{1}{1-\phi} - 2\chi_{PS} + \chi - \alpha(k)p^2\Big)\Big]^2\Big\}$$

where $\alpha(k) = N/(\bar{\epsilon}k^2 + cp\phi N + 2c_sN)$ if we assume that one salt molecule generates one cation and one anion, and $c = 1$ when both the A and B polymers have the smeared charge distribution and $2 - p$ when both the A and B have the annealed charge distribution. Solving the generalized spinodal equations $(\partial S_{AA}/\partial k)|_{k_m,\chi_m} = 0$ and $S_{AA}^{-1}(k_m,\chi_m) = 0$, we obtain

$$k_m^2 = \left(\sqrt{\frac{\phi}{\bar{\epsilon}\dfrac{dP^{-1}}{dk^2}\Big|_{k^2_m}}} - \frac{c\phi}{\bar{\epsilon}}\right)Np - \frac{2c_sN}{\bar{\epsilon}}$$

$$\chi_m = \frac{2P_m^{-1}}{\phi N} + 2\alpha_m p^2$$

where P_m and α_m denote $P(k_m^2)$ and $\alpha(k_m)$, respectively.

If we approximate the polymer form factor by $P(k^2) \approx 1/(1 + bk^2)$, where $1/3 \le b \le 1/2$ is a constant, the above results can then be simplified as

$$k^2{}_m = \left(\sqrt{\frac{\phi}{b\bar{\epsilon}}} - \frac{c\phi}{\bar{\epsilon}}\right)Np - \frac{2c_sN}{\bar{\epsilon}}$$

$$\chi_m = \frac{2}{\phi N} + 2\left[\left(2\sqrt{\frac{b}{\bar{\epsilon}\phi}} - \frac{bc}{\bar{\epsilon}}\right)p - \frac{2bc_s}{\bar{\epsilon}\phi}\right]$$

from which we can see the effects of dielectric constants clearly. In the case where both the A and B polymers have the smeared charge distribution and $c_s = 0$, the critical point of macroscopic phase separation is given by

$$\chi_c = \frac{2}{\phi N} + \frac{2}{\phi}p$$

Therefore, to have microphase separation, $k_m^2 > 0$ and $\chi_m < \chi_c$ are required, which give $\bar{\epsilon} > b\phi$ in this case.

References and Notes

(1) Hara, M. *Polyelectrolytes: Science and Technology*, Marcel Dekker: New York 1993. Dautzenberg, H.; Jaeger, W.; Kotz, J.; Philipp, B.; Seidel, Ch.; Stscherbina, D. *Polyelectrolytes: Formation, Characterization and Application*, Hanser Gardner: Munich, 1994.

(2) Frenkel, D.; Smit, B. *Understanding Molecular Simulation: From Algorithms to Applications*, 2nd ed.; Academic: San Diego, 2002.

(3) Ganesan, V.; Fredrickson, G. H. *Europhys. Lett.* **2001**, *55*(6), 814.

(4) Fredrickson, G. H.; Ganesan, V.; Drolet, F. *Macromolecules* **2002**, *35*(1), 16.

(5) Edwards, S. F. *Proc. Phys. Soc.* **1965**, *85*, 613.

(6) Helfand, E.; Tagami, Y. *J. Polym. Sci., Part B* **1971**, *9*, 741. Helfand, E.; Tagami, Y. *J. Chem. Phys.* **1972**, *56*(7), 3592. Helfand, E.; Tagami, Y. *J. Chem. Phys.* **1972**, *57*(4), 1812.

(7) Helfand, E. *J. Chem. Phys.* **1975**, *62*(3), 999. Helfand, E.; Sapse, A. M. *J. Chem. Phys.* **1975**, *62*(4), 1327. Hong, K. M.; Noolandi, J. *Macromolecules* **1981**, *14*(3), 727 **1981**. Hong, K. M.; Noolandi, J. *Macromolecules* **1981**, *14*(3), 736. Noolandi, J.; Hong, K. M. *Macromolecules* **1982**, *15*(2), 482. Noolandi, J.; Hong, K. M. *Macromolecules* **1984**, *17*(8), 1531. Shull, K. R.; Kramer, E. J. *Macromolecules* **1990**, *23*(22), 4769. Shull, K. R. *Macromolecules* **1993**, *26*(9), 2346.

(8) Whitmore, M. D.; Vavasour, J. D. *Acta Polymer.* **1995**, *46*, 341.

(9) Matsen, M. W.; Bates, F. S. *Macromolecules* **1996**, *29*(4), 1091.

(10) Fleer, G. J.; Cohen Stuart, M. A.; Scheutjens, J. M. H. M.; Cosgrove, T.; Vincent, B. *Polymers at Interfaces*, Chapman & Hall: London 1993. Fleer, G. J.; Leermakers, F. A. M. *Curr. Opin. Colloid Interface Sci.* **1997** *2*(3), 308.

(11) For a recent review of SCF theory, see Schmid, F. *J. Phys.: Condens. Matter* **1998**, *10*, 8105.

(12) Borukhov, I.; Andelman, D.; Orland, H. *Eur. Phys. J. B* **1998**, *5*, 869.

(13) Netz, R. R.; Andelman, D. *Phys. Rep.* **2003**, *380*, 1.

(14) Shi, A.-C.; Noolandi, J. *Macromol. Theory Simul.* **1999**, *8*(3), 214.

(15) Rabin, Y.; Marko, J. F. *Macromolecules* **1991**, *24*(8), 2134.

(16) Benmouna, M.; Vilgis, T. A. *Macromolecules* **1991**, *24*(13), 3866.

(17) Marko, J. F.; Rabin, Y. *Macromolecules* **1992**, *25*(5), 1503.

(18) Benmouna, M.; Vilgis, T. A.; Francois, J. *Makromol. Chem. Theory Simul.* **1992**, *1*, 3.

(19) Benmouna, M.; Bouayed, Y. *Macromolecules* **1992**, *25*(20), 5318.

(20) Gonzalez-Mozuelos, P.; Olvera de la Cruz, M. *J. Chem. Phys.* **1994**, *100*(1), 507.

(21) Banaszak, M.; Clarke, J. H. R. *Phys. Rev. E* **1999**, *60*(5), 5753.

(22) Borue, V. Yu.; Erukhimovich, I. Ya. *Sov. Phys. Dokl.* **1986**, *31*(2), 146.

(23) Nyrkova, I. A.; Khokhlov, A. R.; Kramarenko, Ye. Yu. *Polym. Sci. USSR* **1990**, *32*(5), 852.

(24) Brereton, M. G.; Vilgis, T. A. *Macromolecules* **1990**, *23*(7), 2044.

(25) Joanny, J. F.; Leibler, L. *J. Phys. France* **1990**, *51*, 545.

(26) Borue, V. Yu.; Erukhimovich, I. Ya. *Macromolecules* **1988**, *21*(11), 3240.

(27) Vilgis, T. A.; Borsali, R. *Phys. Rev. A* **1991**, *43*(12), 6857.

(28) Benmouna, M.; Vilgis, T. A.; Hakem, F.; Negadi, A. *Macromolecules* **1991**, *24*(24), 6418.

(29) Khokhlov, A. R.; Nyrkova, I. A. *Macromolecules* **1992**, *25*(5), 1493.

(30) Benmouna, M.; Aziz, S.; Vilgis, T. A. *J. Polym. Sci.: Part B: Polym. Phys.* **1993**, *31*, 587.

(31) Benmouna, M.; Hakem, F. I.; Vilgis, T. A. *Ber. Bunsen-Ges. Phys. Chem.* **1996**, *100*(6), 815.

(32) Leibler, L. *Macromolecules* **1980**, *13*(6), 1602.

(33) Dormidontova, E. E.; Erukhimovich, I. Ya.; Khokhlov, A. R. *Macromol. Theory Simul.* **1994**, *3*, 661.

(34) Dobrynin, A. V.; Erukhimovich, I. Ya. *Sov. Phys. JETP* **1991**, *72*(4), 751.

(35) Nyrkova, I. A.; Khokhlov, A. R.; Doi, M. *Macromolecules* **1994**, *27*(15), 4220.

(36) Tang, H.; Freed, K. F. *J. Chem. Phys.* **1991**, *94*(9), 6307.

(37) This is correct at the mean-field level. For example, in the case of weak polyacids carrying monovalent charges, the probability ratio between the dissociated and nondissociated states of a dissociable segment is given by $10^{pH-pK_0} \times \exp(-\Delta\mathscr{U})$, where K_0 is the intrinsic segmental dissociation constant and $\Delta\mathscr{U}$ is the energy difference (in units of k_BT) between the two states;[38] the mean-field theory does not distinguish the dissociation between the polyacid and the corresponding monomeric acid, and thus gives $\alpha_P/(1 - \alpha_P) = 10^{pH-pK_0}$.[39]

(38) See, for example, Reed, C. E.; Reed, W. F. *J. Chem. Phys.* **1992**, *96*(2), 1609.

(39) See, for example, Borukhov, I.; Andelman, D.; Borrega, R.; Cloitre, M.; Leibler, L.; Orland, H. *J. Phys. Chem. B* **2000**, *104*(47), 11027.

(40) Netz, R. R.; Orland, H. *Eur. Phys. J. E* **2000**, *1*, 203.

(41) $2m$ of these equations correspond to eqs 15 and 16; the rest $(m_P - 1)m$ equations correspond to, say, $\omega_P - \omega_A + \chi_{AP}N(\phi_P - \phi_A) - (\chi_{PS} - \chi_{AS})N(\mathbf{1} - \sum_{P'}\phi_{P'}) - \sum_{P'\neq A,P}(\chi_{PP'} - \chi_{AP'})N\phi_{P'} = 0$ for $P \neq A$. During each iteration, ϕ_P and $\phi_\pm$ are calculated from eq 17 and eqs 12−14, then ω_S is calculated as $\omega_S = \omega_A + \chi_{AS}N(2\phi_A - \mathbf{1}) + \sum_{P\neq A}(\chi_{AS} + \chi_{PS} - \chi_{AP})N\phi_P$, and finally ϕ_S is calculated from eq 14.

(42) Broyden, C. G. *Math. Comput.* **1965**, *19*(92), 577.

(43) Tzeremes, G.; Rasmussen, K. O.; Lookman, T.; Saxena, A. *Phys. Rev. E* **2002**, *65*(4), 041806.

(44) http://www.fftw.org/.

(45) *Numerical Recipes in C: the Art of Scientific Computing*; Press, W. H. et al., Eds.; Cambridge University Press: New York, 1997; Chapter 12.3.

(46) Shi, A.-C., private communication.